Los Alamos
NATIONAL LABORATORY
memorandum

Los Alamos Neutron Science Center, LANSCE-1
Accelerator Physics and Engineering Group

To/MS: Distribution
From/MS: R. W. Garnett, LANSCE-1, H817
Phone/Fax: 5-2835/5-2904
Symbol: LANSCE-1:99-053
Date: March 23, 1999
Email: rgarnett@lanl.gov

SNS 1-TANK DTL INPUT BEAM MIS-STEERING AND MISMATCH SENSITIVITY STUDY

I. Introduction

A study was done to determine the input beam mis-steering and input beam mismatch sensitivities for the SNS 1-Tank DTL. Additionally, this study was done to determine the feasibility of measuring various levels of mis-steering or mismatch at injection to the DTL using diagnostics placed in the CCDTL. All simulations were done for the 2 MW case only.

The input beam to the DTL was generated using the optimized 18-quad baseline MEBT as described in another memorandum. No alignment or other errors were generated in the MEBT in the simulation. Particle distributions having 10,000 macroparticles and a peak current of 56 mA were used for each simulation run.

For the mis-steering calculations, an initial particle distribution was generated and transported through the RFQ with no errors using the code, PARMULT. This same starting distribution was used for all runs transported through the MEBT with either an angle or position displacement of the particle distribution introduced at the end of the MEBT. The beam was then transported through the DTL and finally through a section of the CCDTL up to a final energy of 100 MeV. Beam centroid angular displacements of the DTL input beam were generated over the range ±50 mrad in both x′ and y′, independently. Beam centroid position displacements were generated over the range ±50 mils in both x and y, independently. The PARMILA code was used to simulate the MEBT and DTL. The LINAC code was used to simulate the CCDTL.

For the mismatch calculations the nominal beam was first transported to the end of the MEBT. This beam was assumed to be the matched beam. Using the matched Twiss parameters (α, β) (for this beam) and assuming a fixed value of α, there are two unique values of β for a given mismatch factor. One value defines a beam mismatched and at a smaller projected size in real space. The other value defines a beam of larger projected size, but of equal mismatch factor. A short computer code was used to determine these two β-values for a given α. For all the simulations presented here, the values of β leading to a larger initial beam size were used. The Twiss parameters for the various cases are shown in Table 1. The TRACE 3-D convention for the mismatch factor is assumed.
In order to generate DTL input particle distributions having specific mismatch factors, a particle distribution transformation code, PSTRANS, was used. This code reads the initial particle distribution and transforms it to a distribution having the desired Twiss parameters, in this case, with a specific mismatch factor. The transformation equations are given below where each pair of phase-space coordinates (xx′,yy′,ϕW) are transformed separately:

$$\begin{pmatrix} x_f \\ x'_f \end{pmatrix} = \sqrt{\frac{\varepsilon_2}{\varepsilon_1}} \begin{pmatrix} \sqrt{\frac{\beta_2}{\beta_1}} & 0 \\ \frac{\alpha_1 - \alpha_2}{\sqrt{\beta_1 \beta_2}} & \sqrt{\frac{\beta_1}{\beta_2}} \end{pmatrix} \begin{pmatrix} x_i \\ x'_i \end{pmatrix}$$

where x_i, x'_i (x_f, x'_f) are the initial (final) phase-space coordinates. The Twiss parameters and emittance with subscript 1 are the initial values of the distribution. Those with subscript 2 are the desired final values. For our case, the initial and final emittances are identical. Using this method rather than generating new uniform input distributions with various mismatches at the DTL entrance preserves the real-space shape of the distribution including any tails that may have developed during propagation through the MEBT. Distributions with mismatch factors ranging from 0.1 (10% mismatch) to 1.0 (100% mismatch) for both transverse and longitudinal phase-space were generated.

Table 1 – Twiss Parameters resulting in specified xx′-, yy′, and longitudinal mismatch factors for a fixed value of α.

XMMF	α	β_1(cm/rad)	β_2(cm/rad)
0.0 (Matched)	-0.3825	68.651	-
0.1	"	82.032	57.453
0.2	"	96.530	48.824
0.3	"	112.150	42.024
0.4	"	128.899	36.563
0.5	"	146.783	32.108
0.8	"	207.315	22.733
1.0	"	253.457	18.595
YMMF	α	β_1(cm/rad)	β_2(cm/rad)
0.0 (Matched)	-0.0622	22.7907	-
0.2	"	32.796	15.838
0.5	"	51.203	10.144
0.8	"	73.962	7.049
1.0	"	90.952	5.711
ZMMF	α	β_1(deg/MeV)	β_2(deg/MeV)
0.0 (Matched)	-0.0496	324.287	-
0.2	"	466.766	225.299
0.5	"	728.956	144.264
0.8	"	1049.325	100.219
1.0	"	1295.235	81.191

II. Results

Figures 1 and 2 show the dependence of the DTL rms output emittances as a function of x' and y' input beam angle offsets. Variations of up to ±2-3 mrad in both angles cause negligible changes in the output emittances. Changes in x' couple primarily to the x- and z-emittances, and changes in y' couple primarily to the y- and z-emittances. Injection angle offsets of ≥ 5 mrad will lead to a minimum of 25% emittance growth in at least one phase-space plane. No beam losses were observed in either the DTL or CCDTL (up to 100 MeV) in the simulations for angle offsets of ≤10 mrad.

Figures 3 through 8 show the beam centroid displacements in the CCDTL as a result of injection angle offsets at the DTL entrance. The data points shown in the figures are calculated at the center of each quadrupole between CCDTL segments. Based on these results and assuming a BPM resolution of 0.019cm (value assumed for previous steering studies) at 20 MeV in the CCDTL, it should be possible to measure the results of ±2 mrad injection steering offsets at numerous locations in the CCDTL.

Figures 9 and 10 show the dependence of the DTL output rms emittances as a function of x and y input beam centroid displacements. Variations of up to ±20 mils in input beam centroid position cause negligible changes in the output emittances. Just as in the case of the injection angle offsets, changes in x-position couple primarily to the x- and z-emittances, and changes in y-position couple primarily to the y- and z-emittances. Input position offsets of ≥ 30 mils will lead to a minimum of 15% emittance growth in at least one phase-space plane. No beam losses were observed in either the DTL or CCDTL (up to 100 MeV) over the full range of position offsets simulated.

Figures 11 through 24 show the beam centroid displacements in the CCDTL resulting from various input beam centroid displacements. Again, based on these results and the previously assumed BPM resolution, it should be possible to measure the results of ± 5 mils input beam centroid displacements using diagnostics placed in the CCDTL near 20 MeV.

Figures 25 through 27 show the dependence of the DTL output rms emittance as a function of input beam mismatch factors. It can readily be seen that for a mismatch factor > 0.5, significant emittance growth begins to occur in all phase-space planes. It should be noted, however, that for mismatches up to 1.0 in both transverse planes, no beam loss in either the DTL or CCDTL was observed. Beam loss was observed in the simulations in the DTL for a longitudinal mismatch factor starting at 0.5. CCDTL beam loss was observed for a longitudinal mismatch factor of 1.0.

Figures 28 through 35 show plots of the x-rms beam size in the CCDTL up to 100 Mev for various values of injected beam mismatch factor. It would be necessary to measure variations in beam envelope size of order 0.01 cm to detect the results of an input beam transverse mismatch factor of 0.2. As can be seen in Figs. 28 and 29, the envelope oscillations for the 0.2 mismatch factor damp out after approximately the first 10 FODO periods in the CCDTL (after quad 20). For a mismatch factor of 0.5, approximately half the resolution is required. This level of mismatch in the yy'-plane appears to have a greater effect on the beam envelope than for the xx'-plane (See Figs. 30-31). Changes in beam envelope size may be resolvable for an xx'-mismatch out to approximately CCDTL segment number 40, whereas the same mismatch in the yy'-plane should be measurable anywhere in the CCDTL.

Figures 34 and 35 show the changes in x-rms beam envelope size in the CCDTL resulting from a mismatch factor of 0.5 in xx′ and yy′ for the small-β values, respectively. These figures should be compared with Figs. 30-31.

Figures 36 through 39 show the rms phase-width of the beam as a function of CCDTL segment number for various longitudinal mismatch values. The rms phase-width is given in units of degrees at F=805 MHz. It appears that a 20% longitudinal mismatch will be undetectable whereas larger mismatches should be measurable. The large excursions in rms phase-width observed in Figures 38 and 39 are the result of a few particles achieving large phase values prior to being lost longitudinally in the simulations.

RWG:amg

Distribution:
T. Bhatia, LANSCE-1, H817
J. Billen, LANSCE-1, H817
B. Blind, LANSCE-1, H817
D. Gilpatrick, LANSCE-1, H817
B. Hartline, LANSCE-DO, H824
A. Jason, LANSCE-1, H817
S. Kurennoy, LANSCE-1, H817
G. Neuschaefer, LANSCE-1, H817
H. Takeda, LANSCE-1, H817
LANSCE-1 File

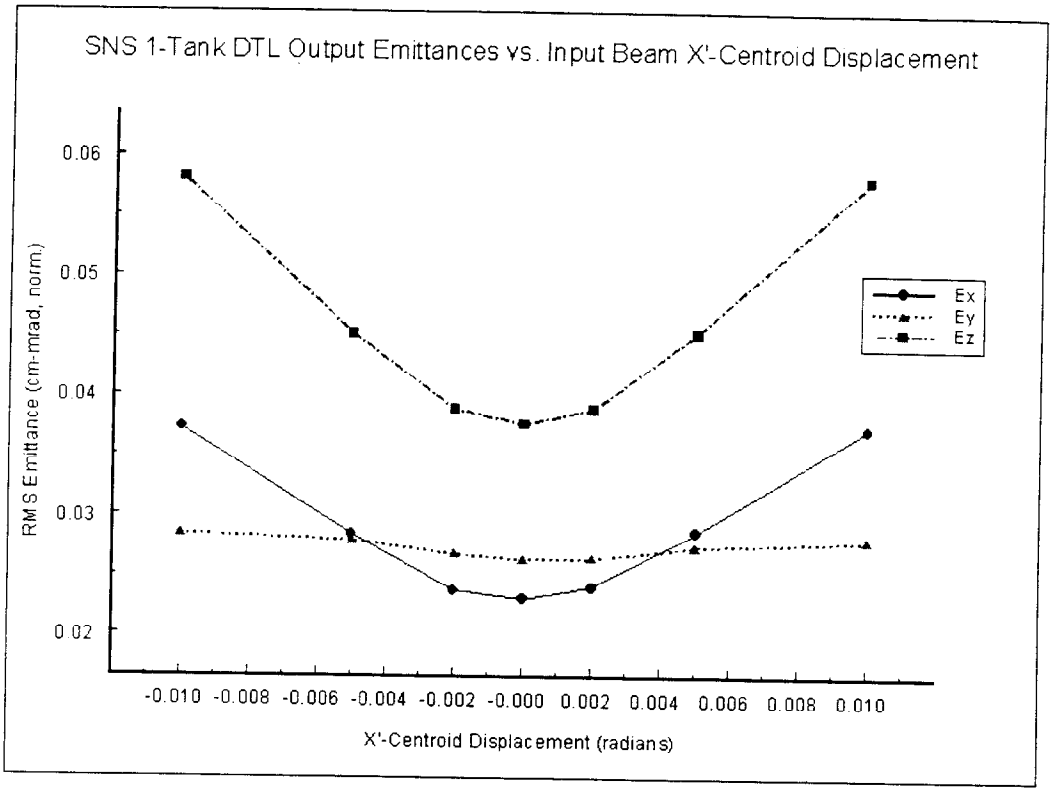

Figure 1 – DTL output emittances as a function of input beam X'-centroid displacement.

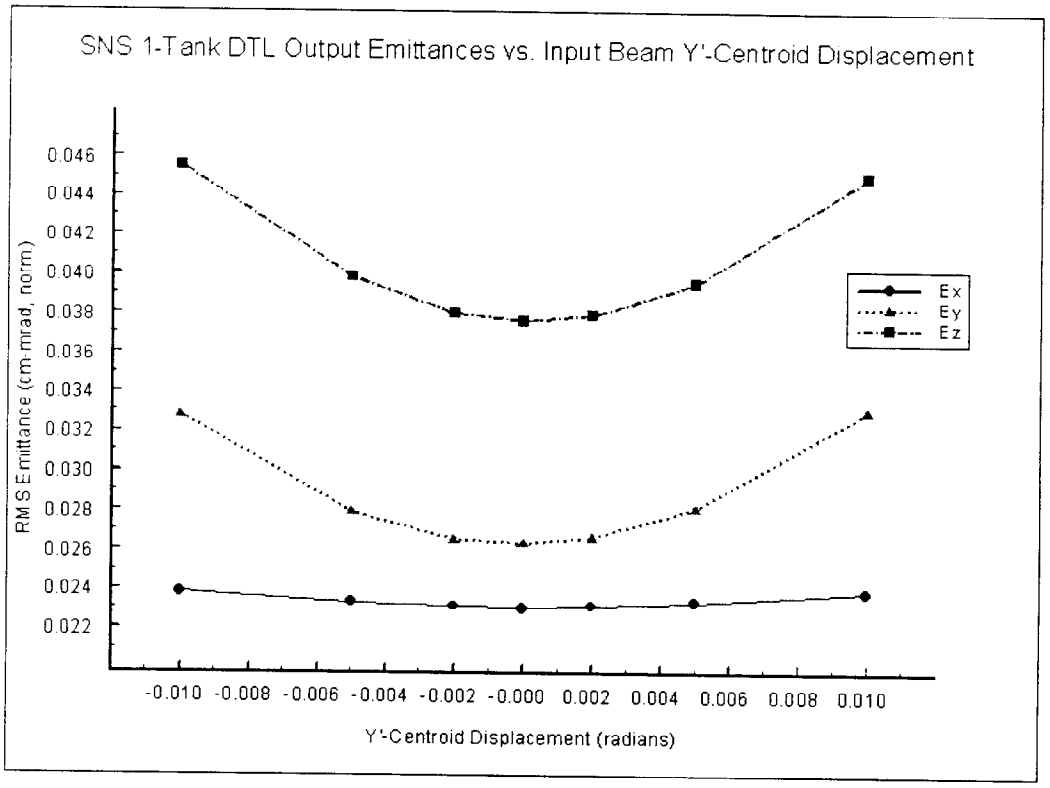

Figure 2 – DTL output emittances as a function of input beam Y'-centroid displacement.

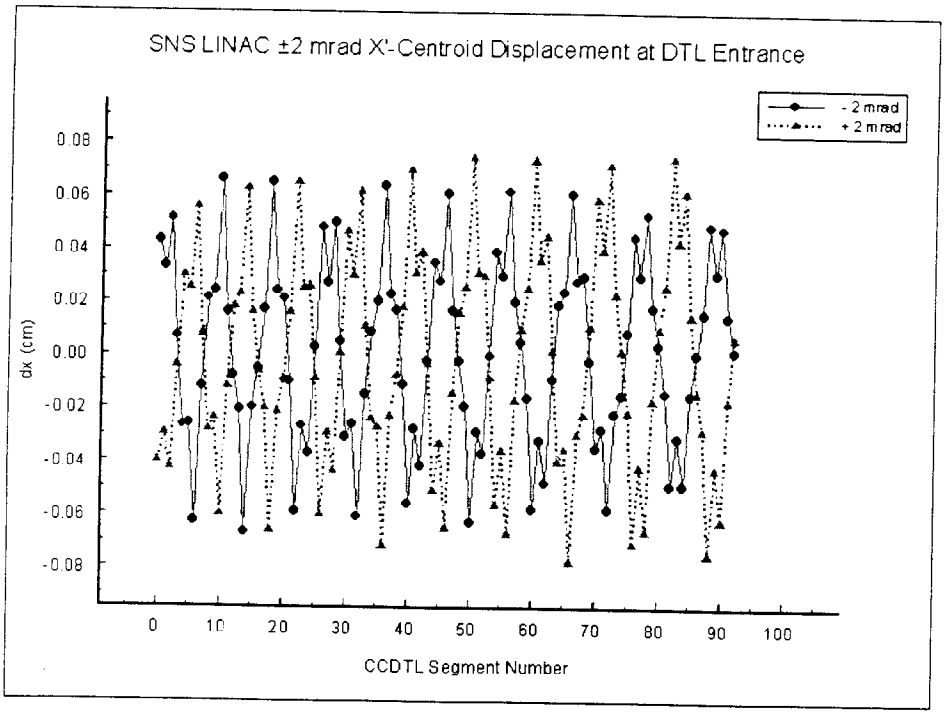

Figure 3 – Beam x-centroid displacements as a function of CCDTL segment number for initial input angle displacements of ±2 mrad.

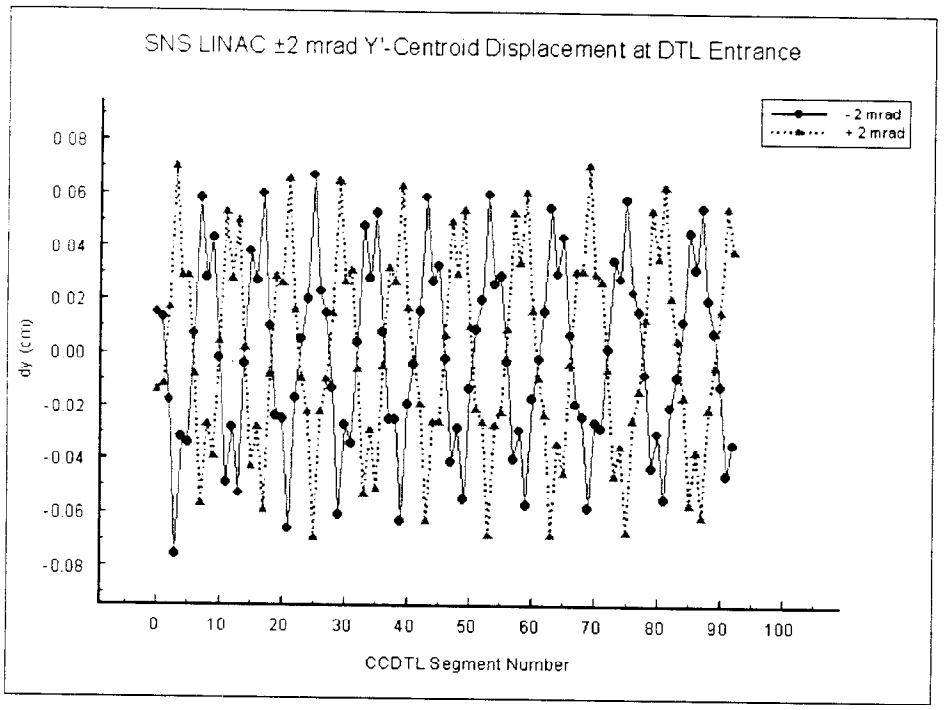

Figure 4 – Beam y-centroid displacements as a function of CCDTL segment number for initial input angle displacements of ±2 mrad.

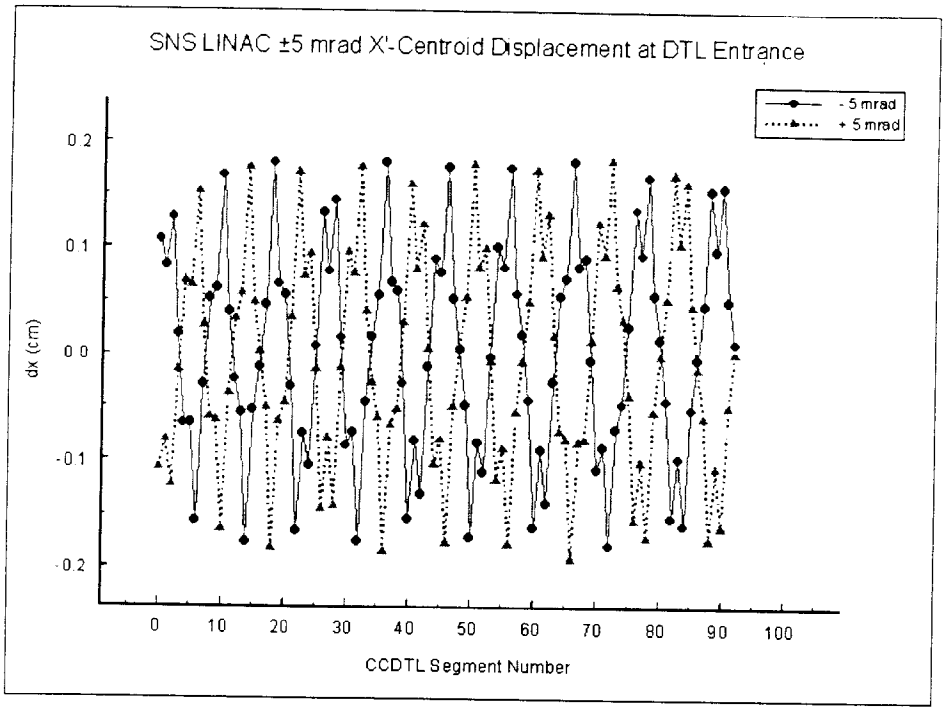

Figure 5 – Beam x-centroid displacements as a function of CCDTL segment number for initial input angle displacements of ±5 mrad.

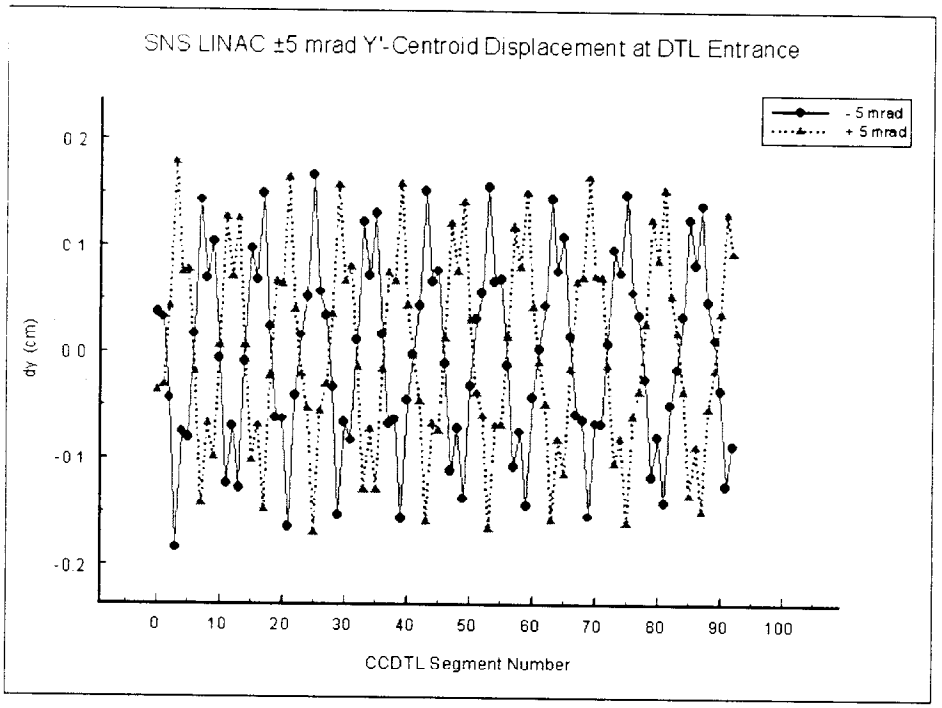

Figure 6 – Beam y-centroid displacements as a function of CCDTL segment number for initial input angle displacements of ±5 mrad.

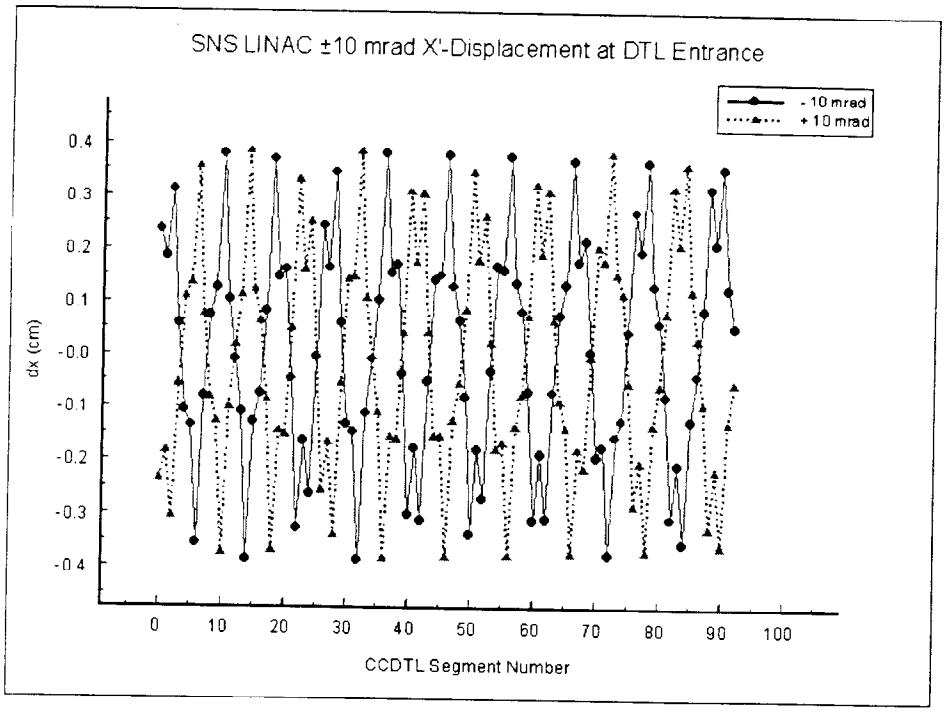

Figure 7 – Beam x-centroid displacements as a function of CCDTL segment number for initial input angle displacements of ±10 mrad.

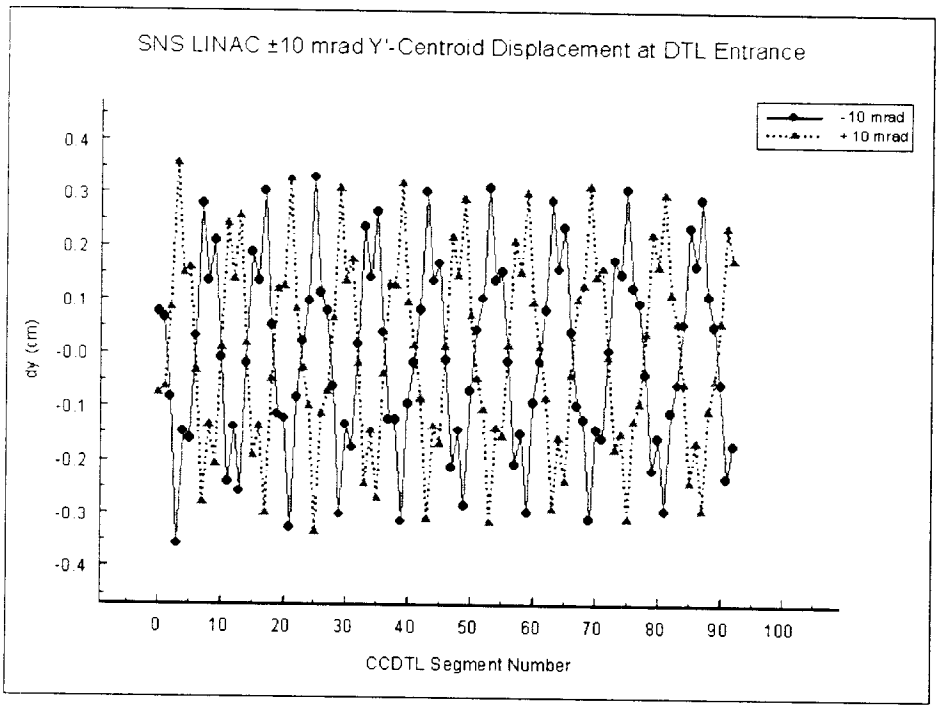

Figure 8 – Beam y-centroid displacements as a function of CCDTL segment number for initial input angle displacements of ±10 mrad.

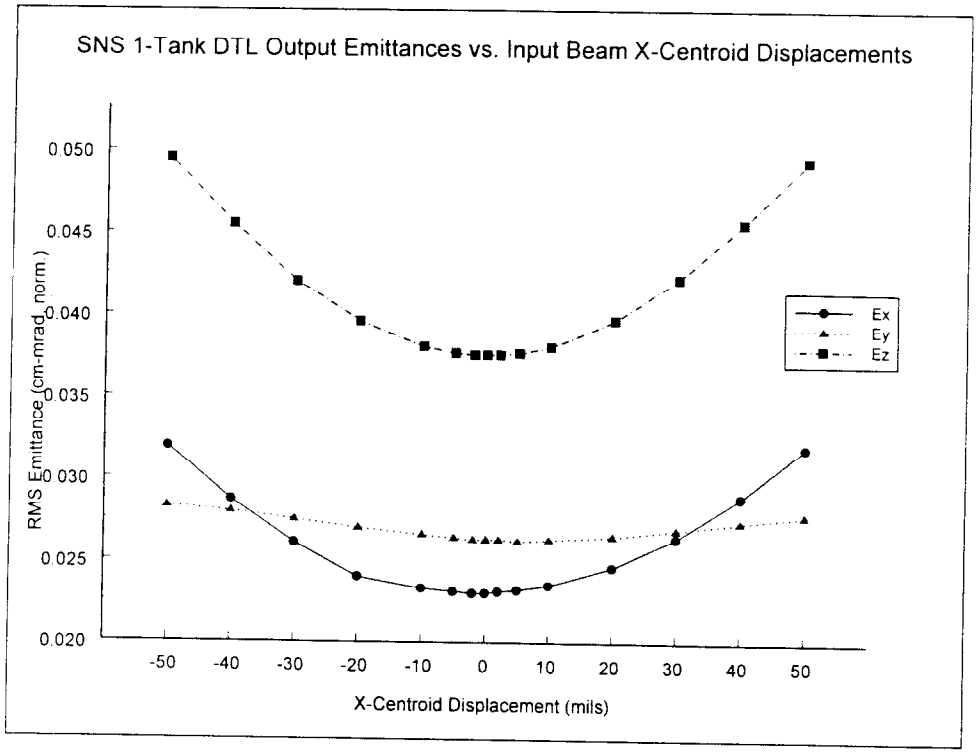

Figure 9 – DTL output emittances as a function of input beam X-centroid displacement.

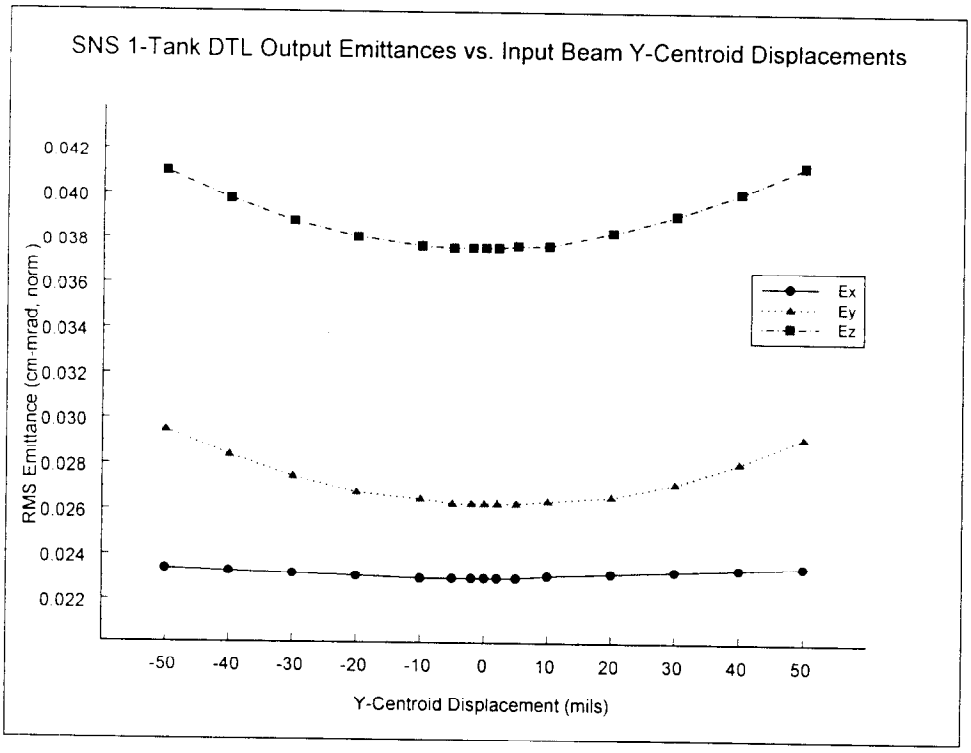

Figure 10 – DTL output emittances as a function of input beam Y-centroid displacement.

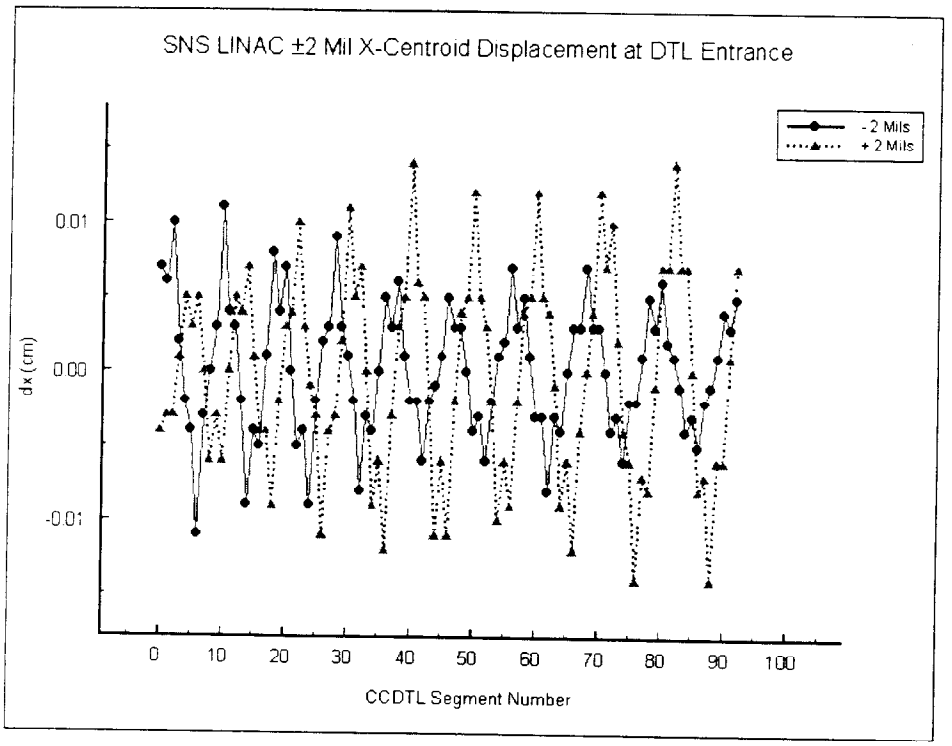

Figure 11 – Beam x-centroid displacements as a function of CCDTL segment number for initial input x-centroid displacements of ±2 mils.

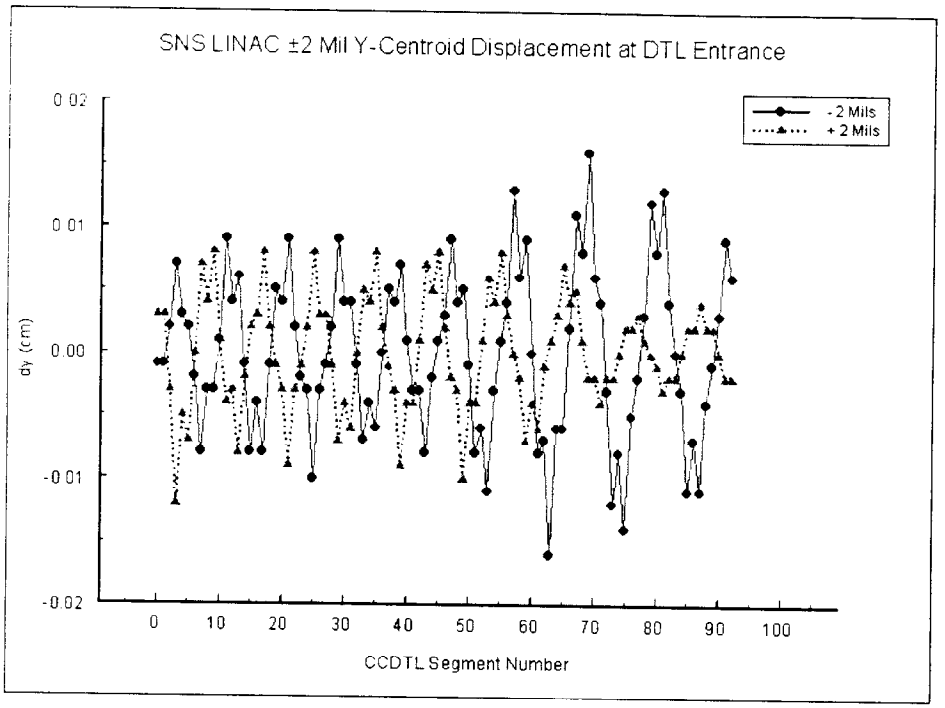

Figure 12 – Beam y-centroid displacements as a function of CCDTL segment number for initial input y-centroid displacements of ±2 mils.

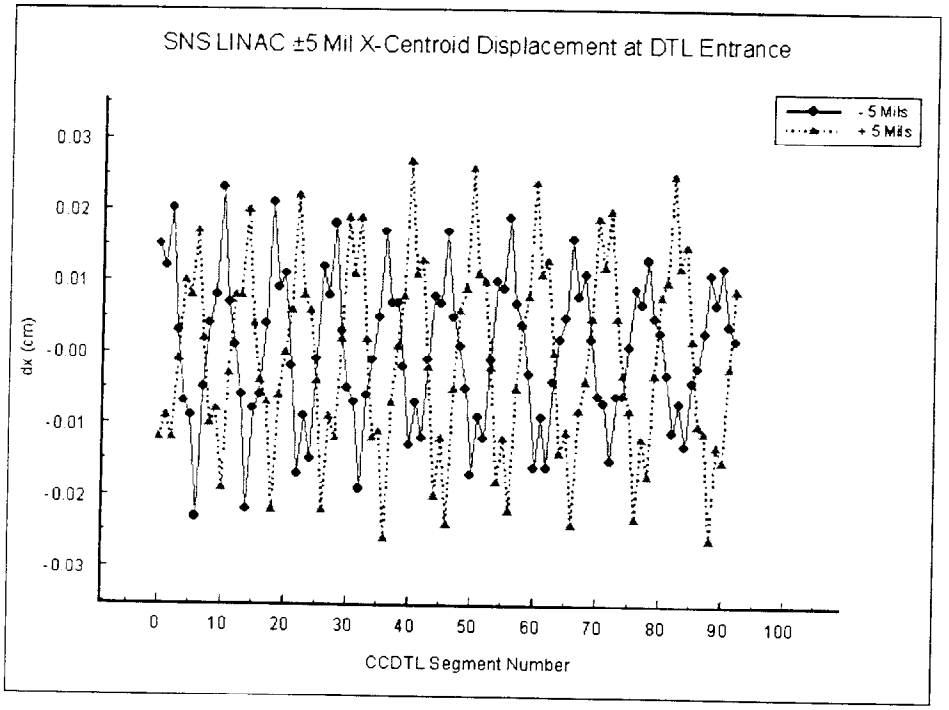

Figure 13 – Beam x-centroid displacements as a function of CCDTL segment number for initial input x-centroid displacements of ±5 mils.

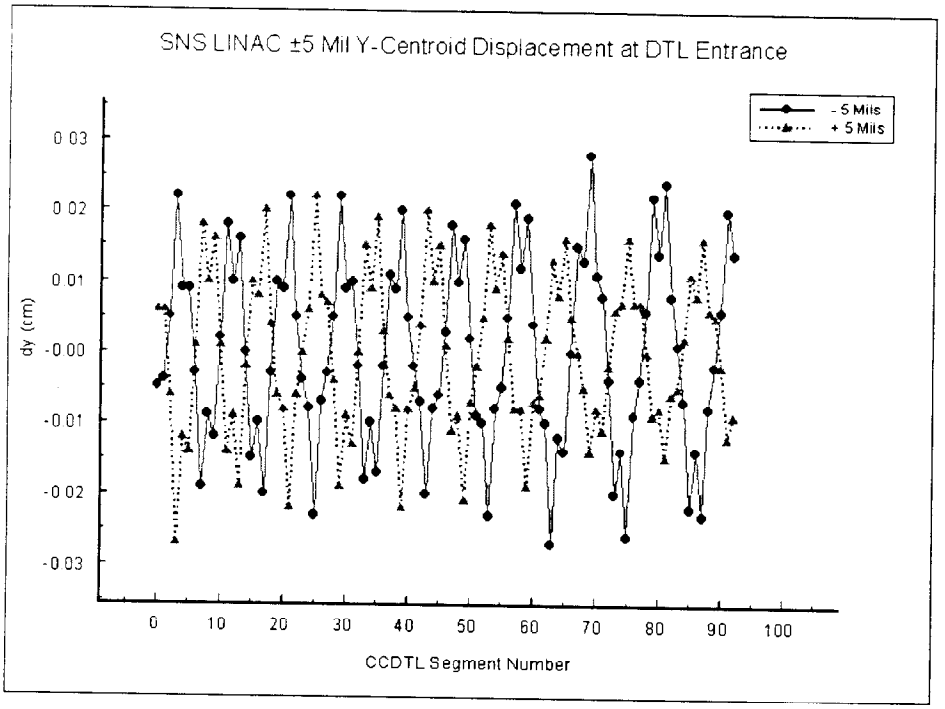

Figure 14 – Beam y-centroid displacements as a function of CCDTL segment number for initial input y-centroid displacements of ±5 mils.

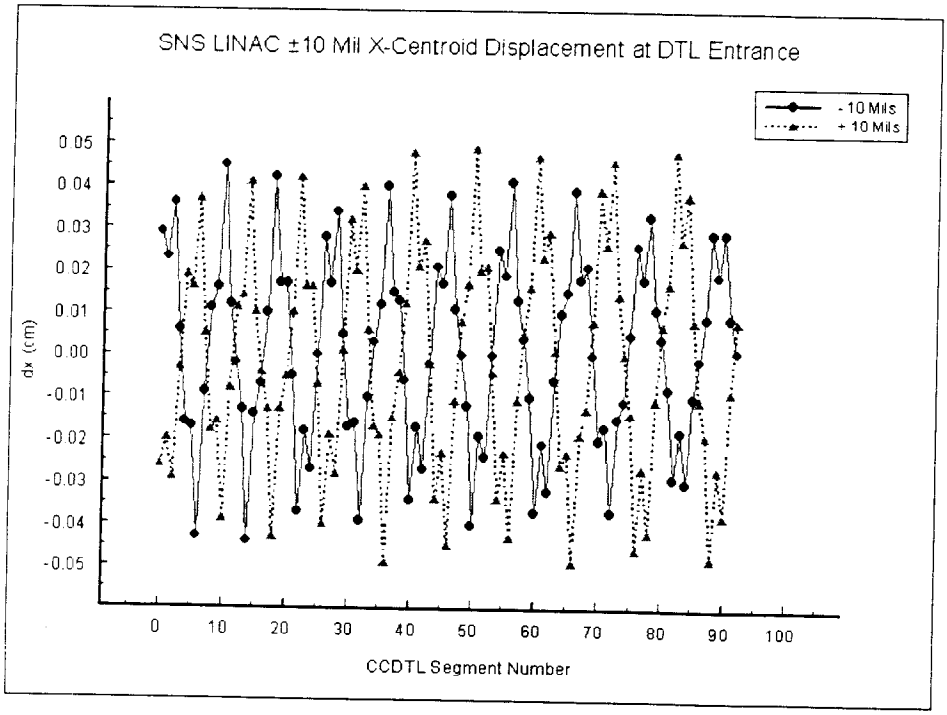

Figure 15 – Beam x-centroid displacement as a function of CCDTL segment number for initial input x-centroid displacements of ±10 mils.

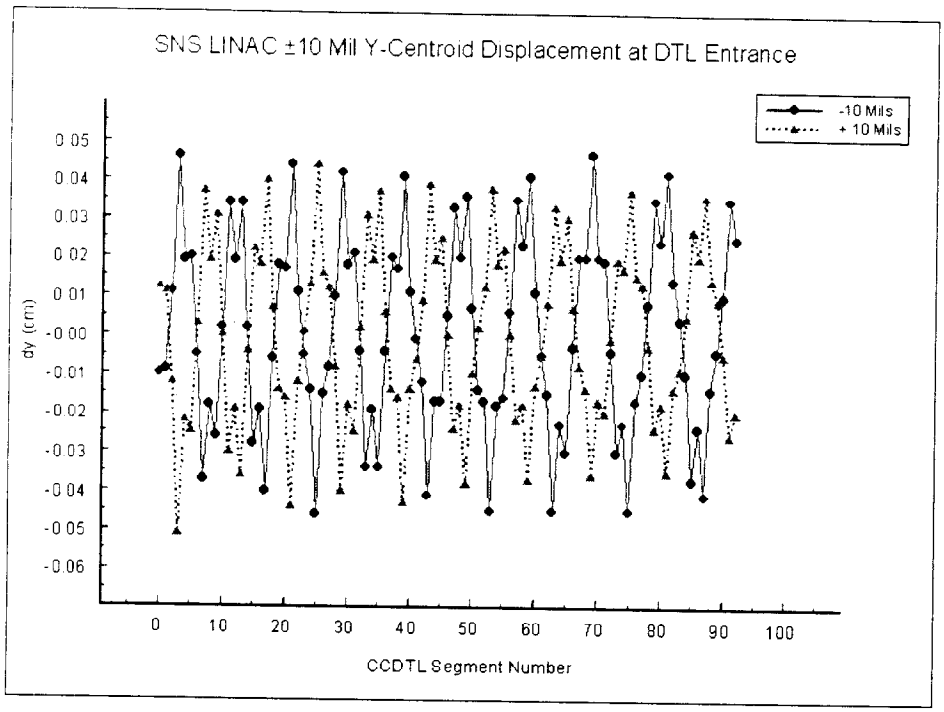

Figure 16 – Beam y-centroid displacement as a function of CCDTL segment number for initial input y-centroid displacements of ±10 mils.

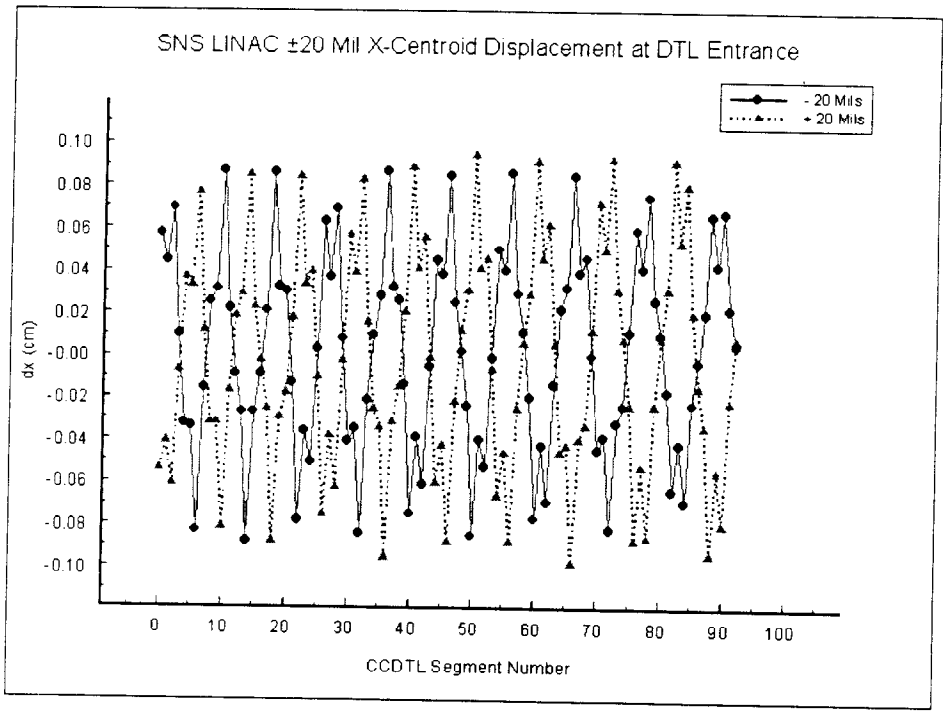

Figure 17 – Beam x-centroid displacement as a function of CCDTL segment number for initial input x-centroid displacements of ±20 mils.

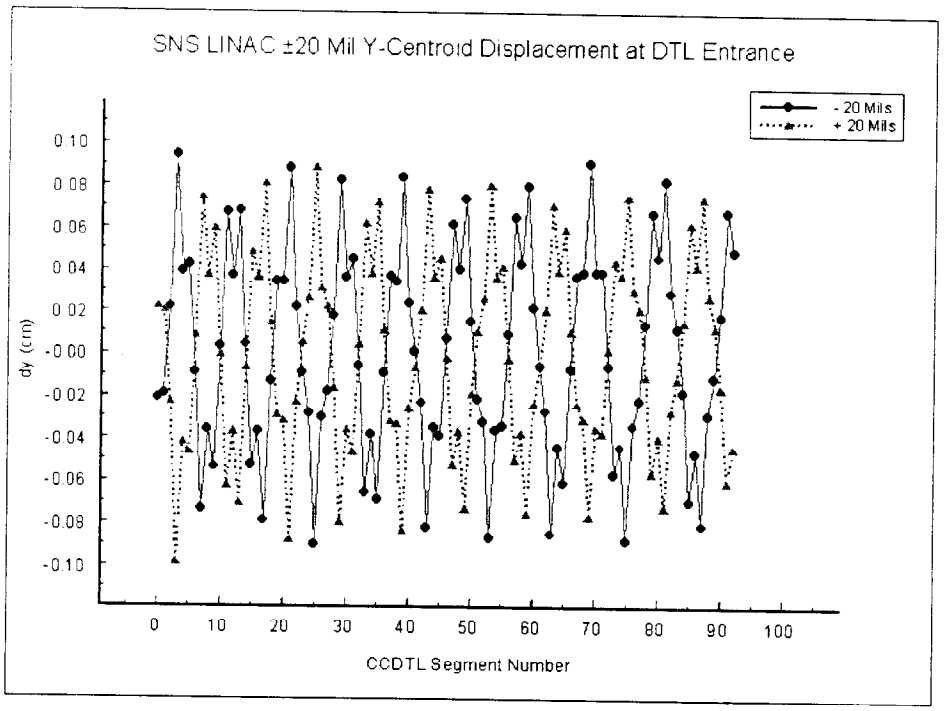

Figure 18 – Beam y-centroid displacement as a function of CCDTL segment number for initial input y-centroid displacements of ±20 mils.

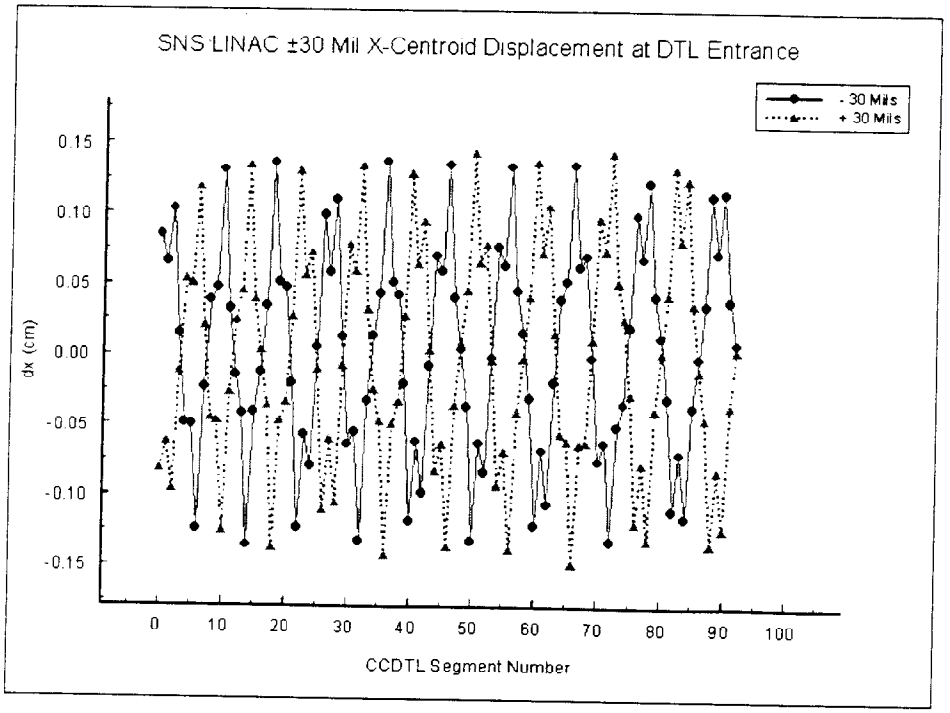

Figure 19 – Beam x-centroid displacement as a function of CCDTL segment number for initial input x-centroid displacements of ±30 mils.

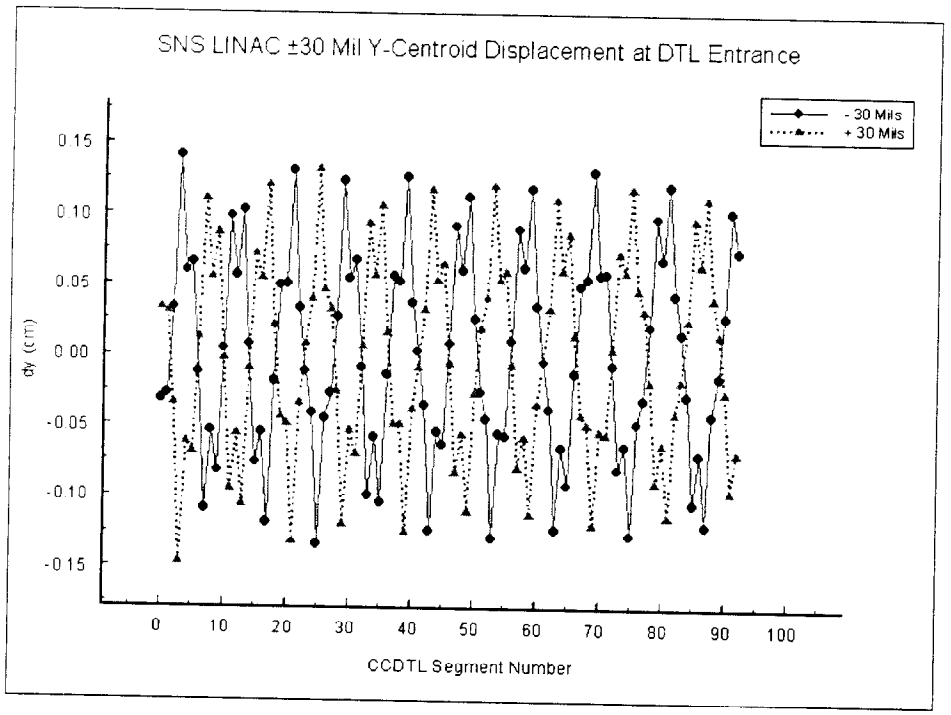

Figure 20 – Beam y-centroid displacement as a function of CCDTL segment number for initial input y-centroid displacements of ±30 mils.

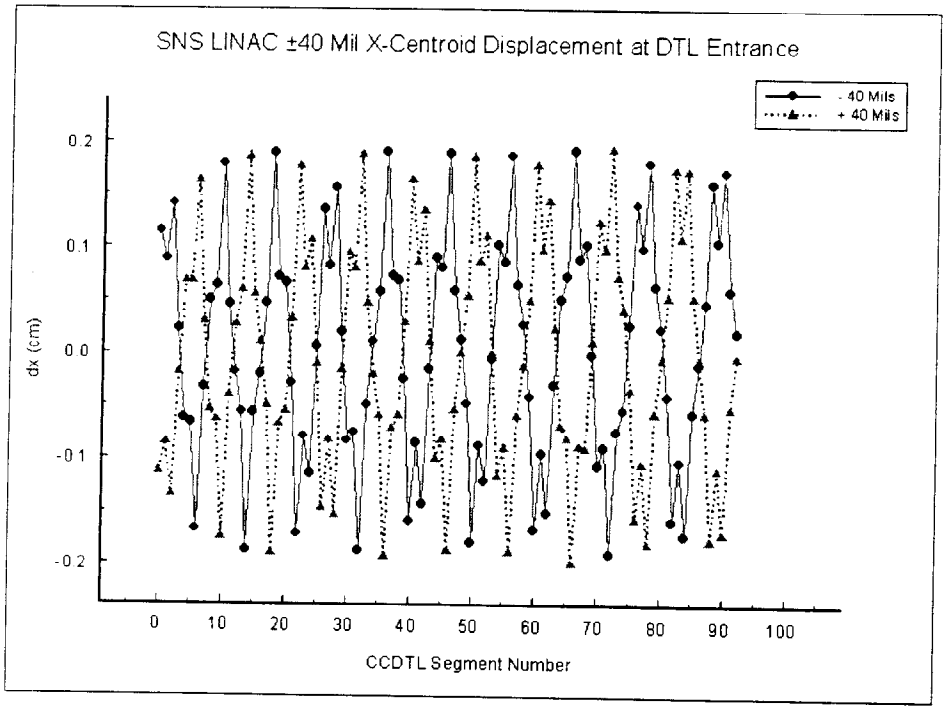

Figure 21 – Beam x-centroid displacement as a function of CCDTL segment number for initial input x-centroid displacements of ±40 mils.

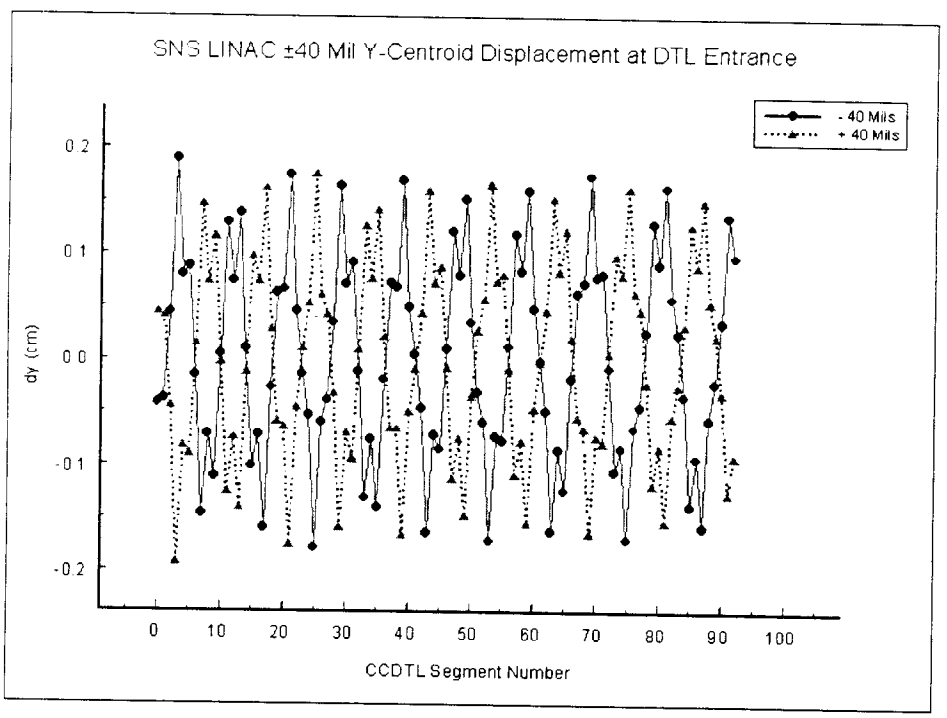

Figure 22– Beam y-centroid displacement as a function of CCDTL segment number for initial input y-centroid displacements of ±40 mils.

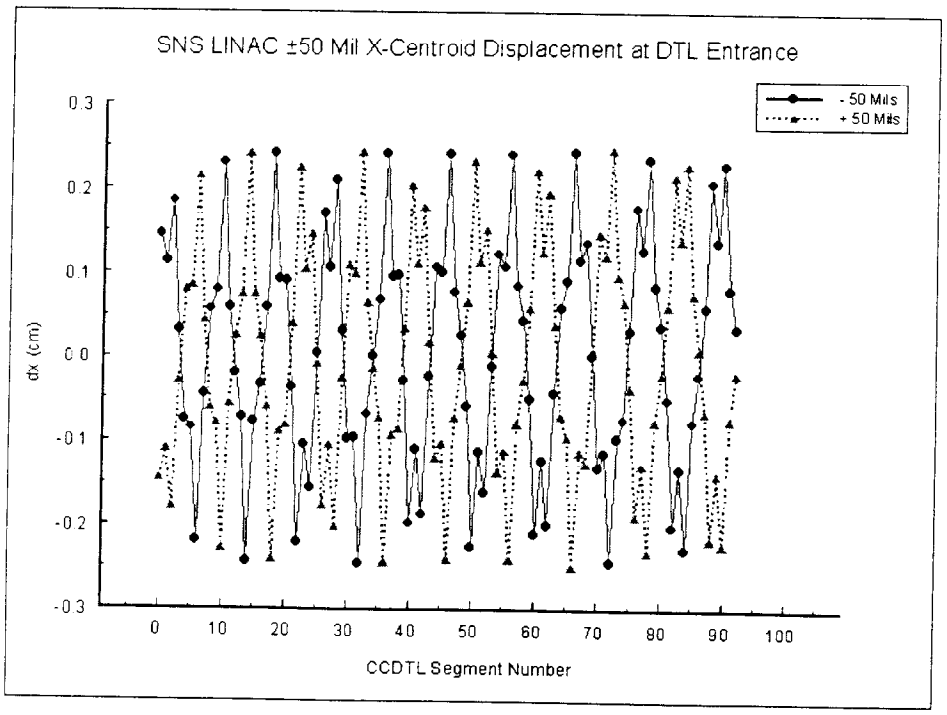

Figure 23 – Beam x-centroid displacement as a function of CCDTL segment number for initial input x-centroid displacements of ±50 mils.

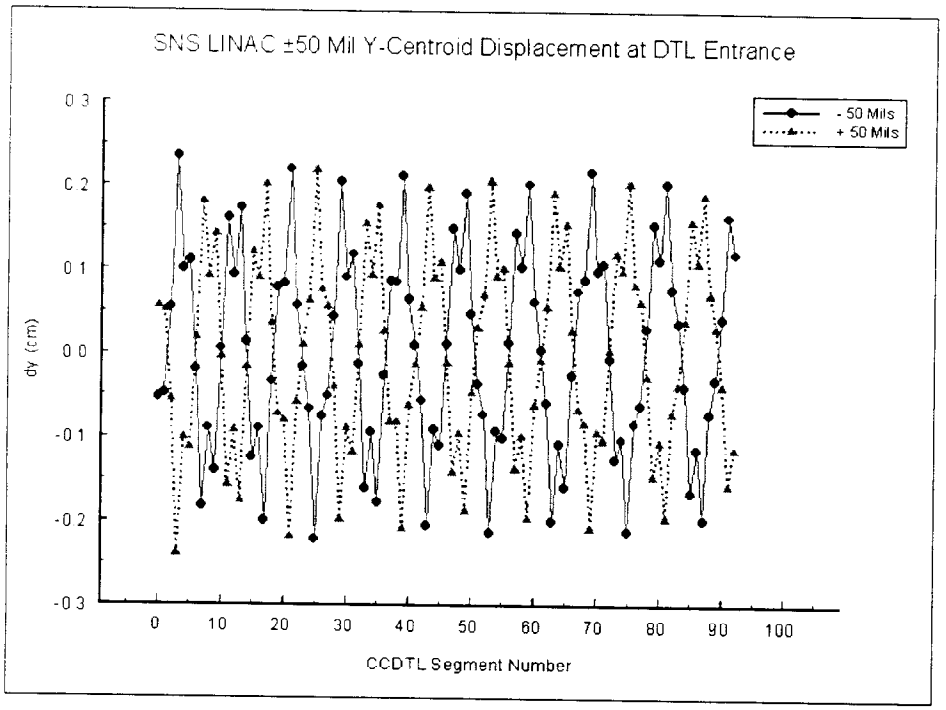

Figure 24 – Beam y-centroid displacement as a function of CCDTL segment number for initial input y-centroid displacements of ±50 mils.

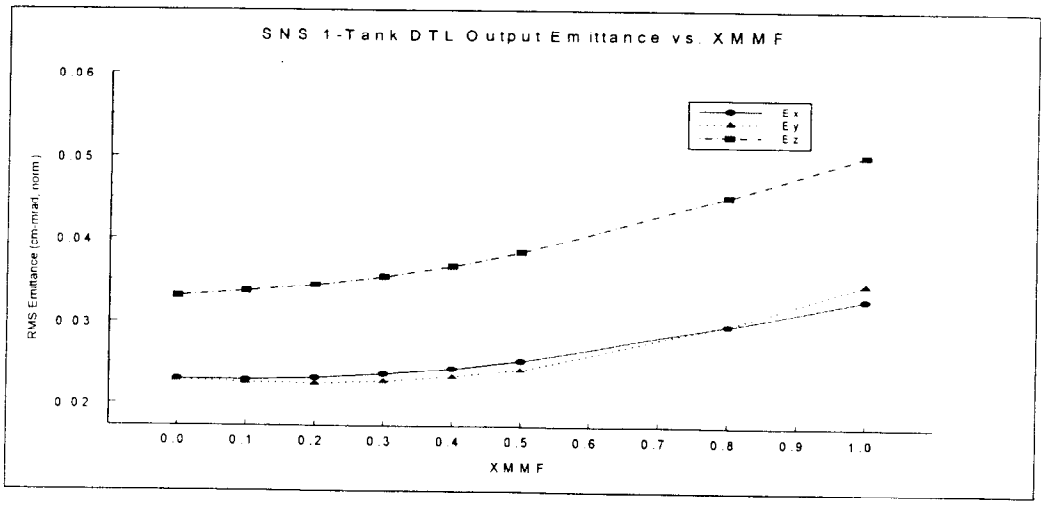

Figure 25 – DTL output rms emittances as a function of input beam x-mismatch factor.

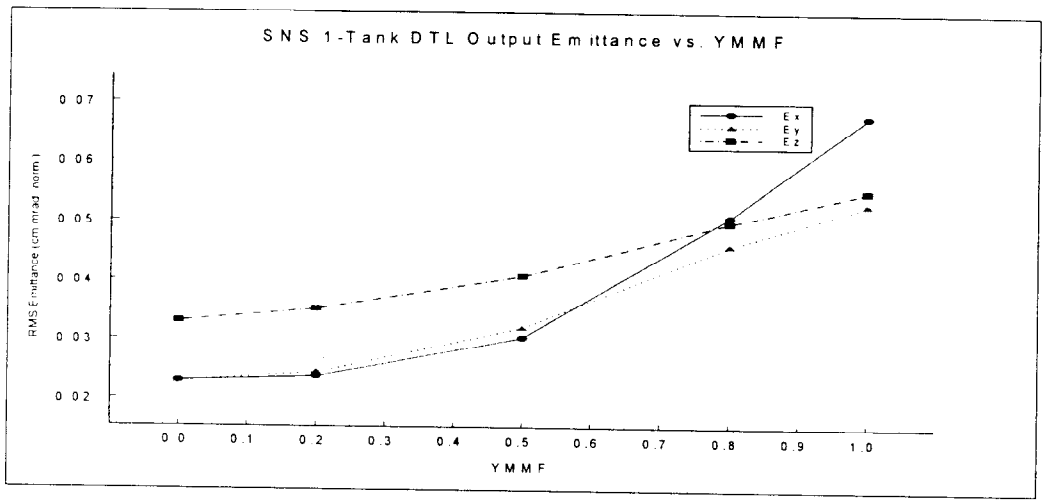

Figure 26 – DTL output rms emittances as a function of input beam y-mismatch factor.

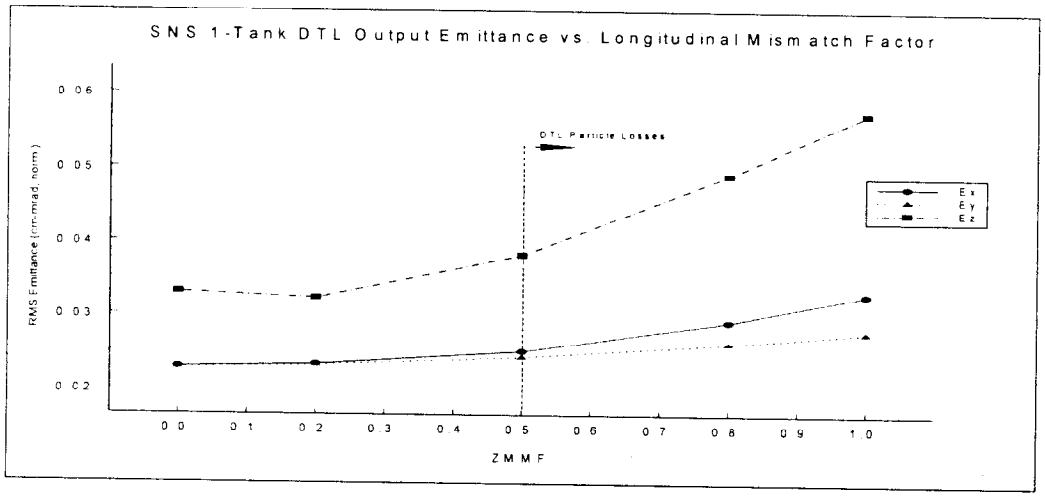

Figure 27 – DTL output rms emittances as a function of input beam z-mismatch factor.

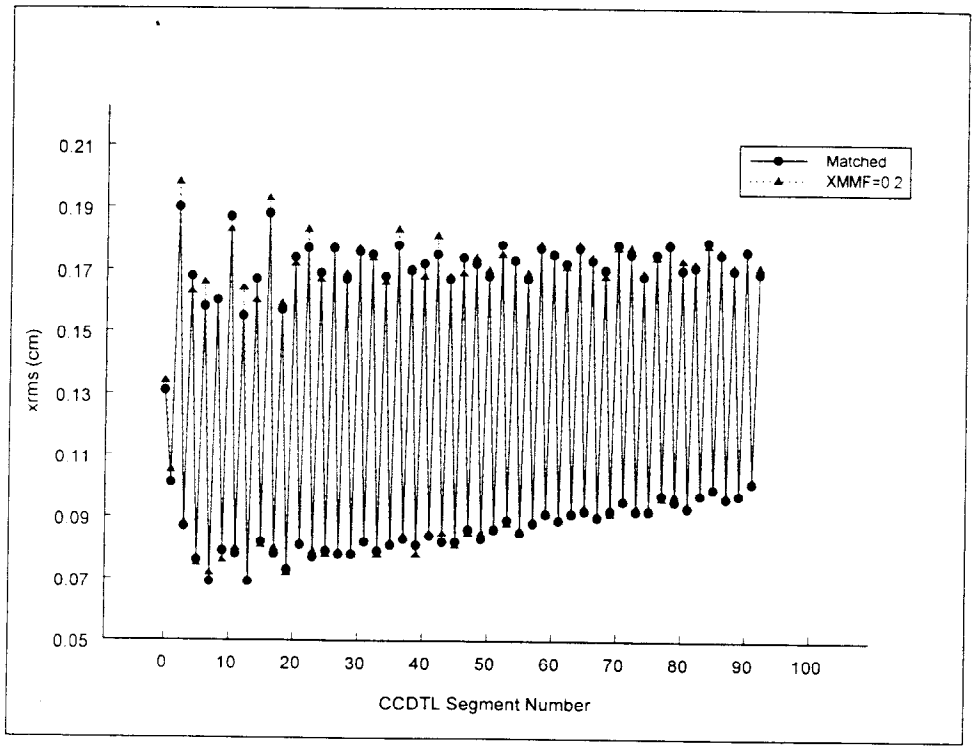

Figure 28 – X-rms beam size as a function of CCDTL segment number for an input beam x-mismatch factor of 0.2.

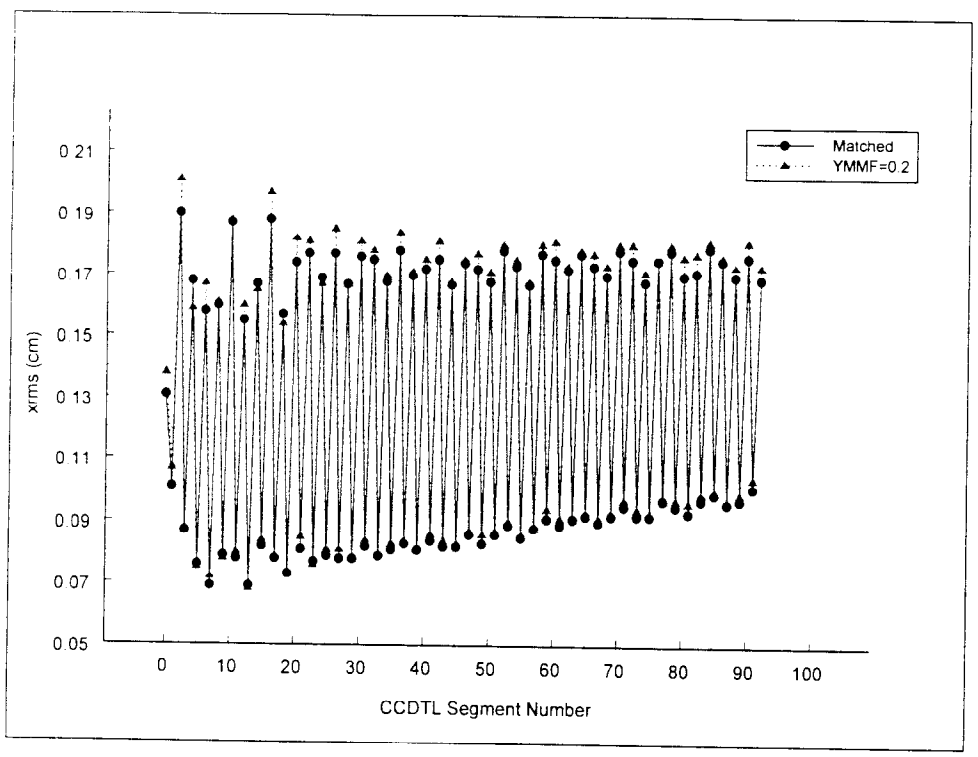

Figure 29 – X-rms beam size as a function of CCDTL segment number for an input beam y-mismatch factor of 0.2

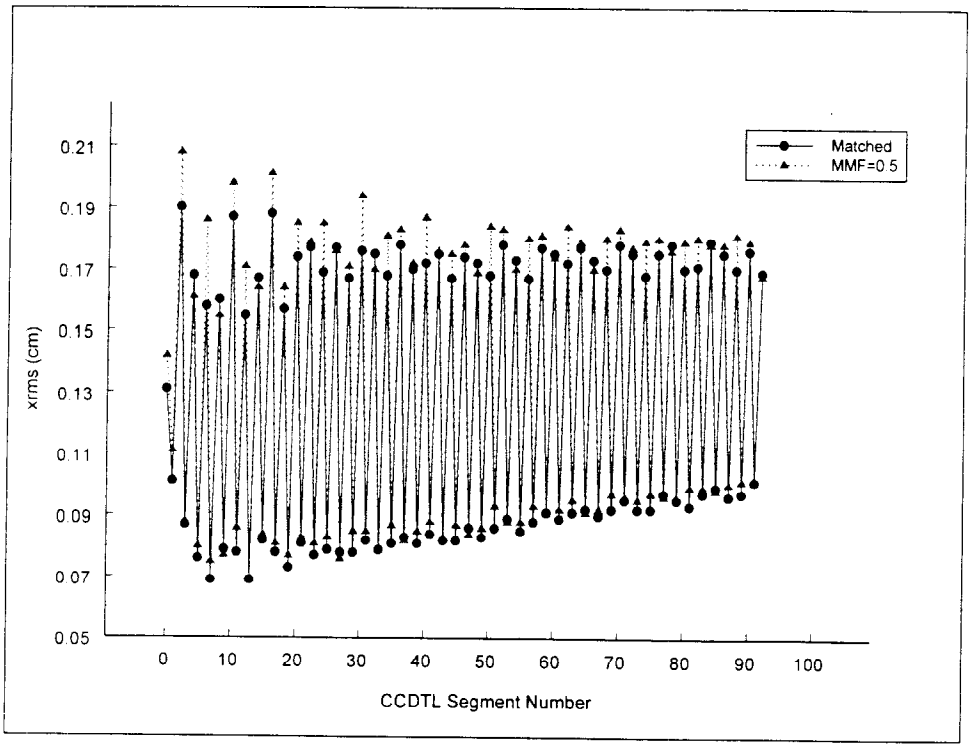

Figure 30 – X-rms beam size as a function of CCDTL segment number for an input beam x-mismatch factor of 0.5.

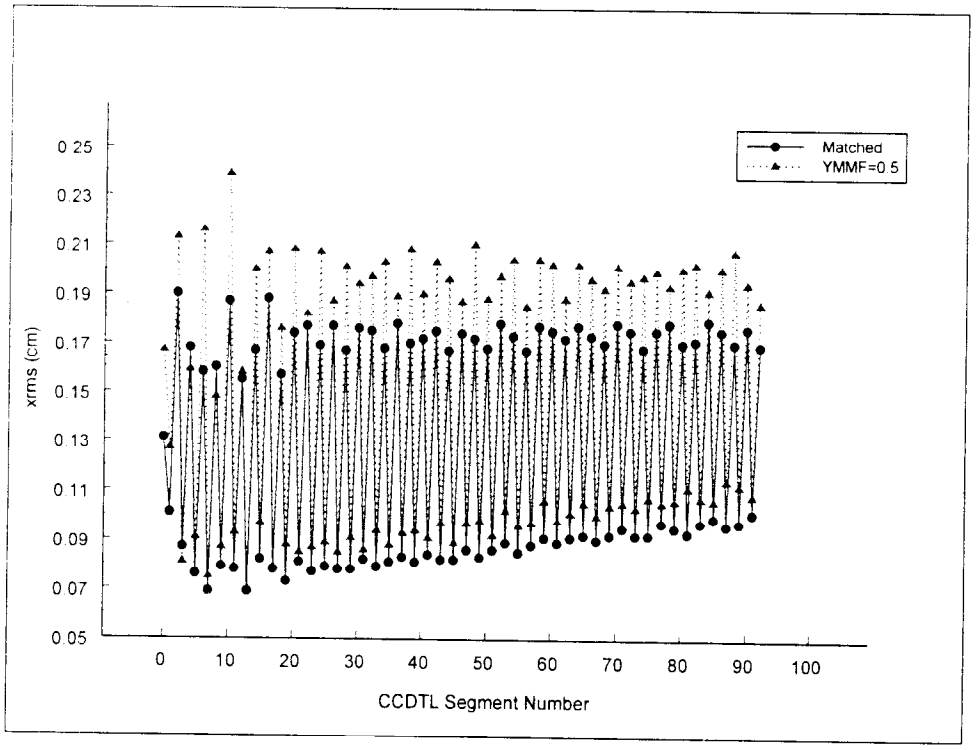

Figure 31 – X-rms beam size as a function of CCDTL segment number for an input beam y-mismatch factor of 0.5.

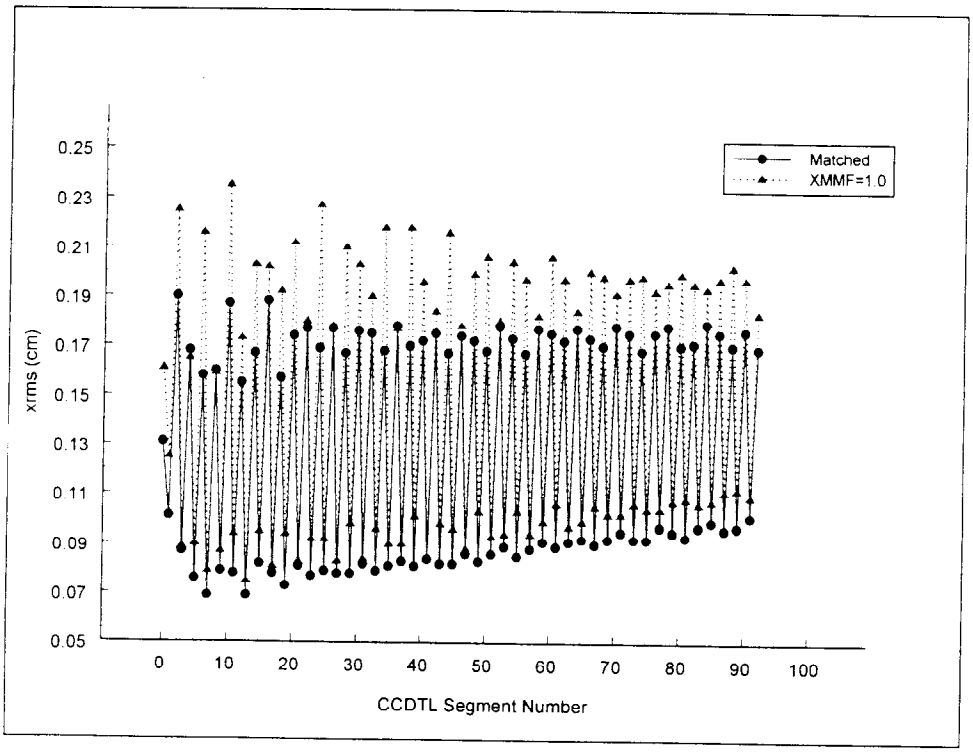

Figure 32 – X-rms beam size as a function of CCDTL segment number for an input beam x-mismatch factor of 1.0.

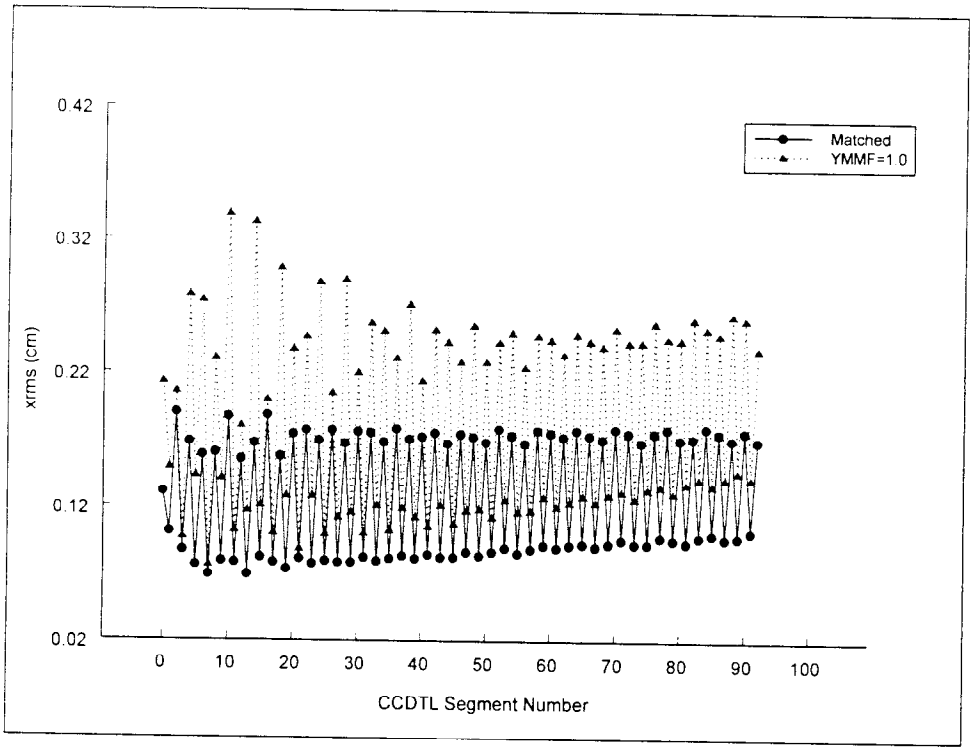

Figure 33 – X-rms beam size as a function of CCDTL segment number for an input beam y-mismatch factor of 1.0.

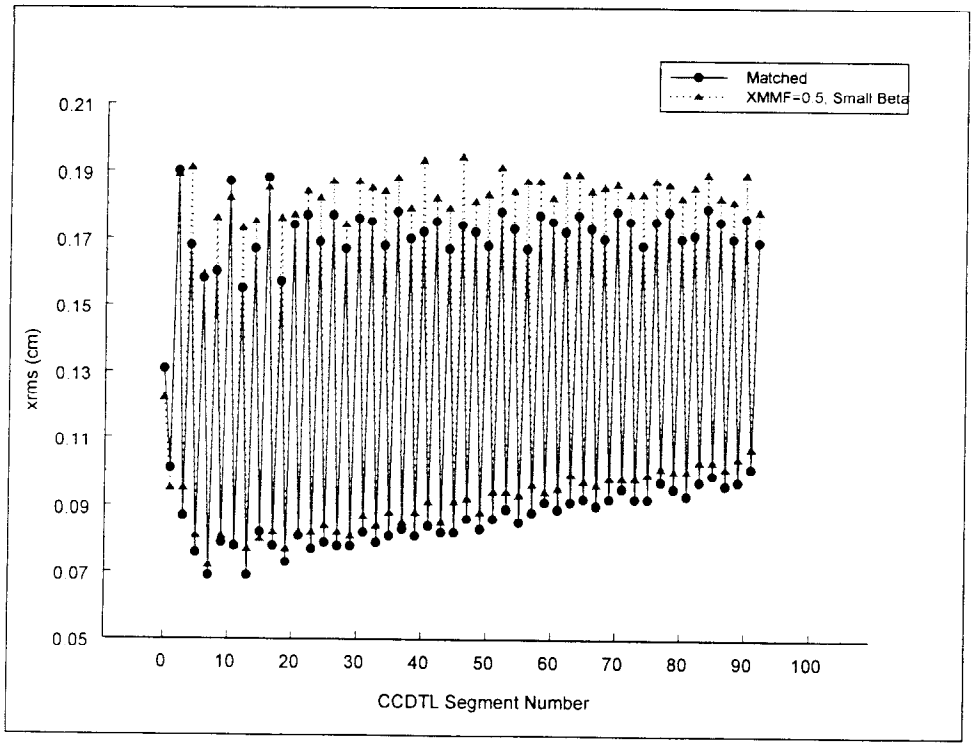

Figure 34 – X-rms beam size as a function of CCDTL segment number for an input beam x-mismatch factor of 0.5 and using the small-β-value.

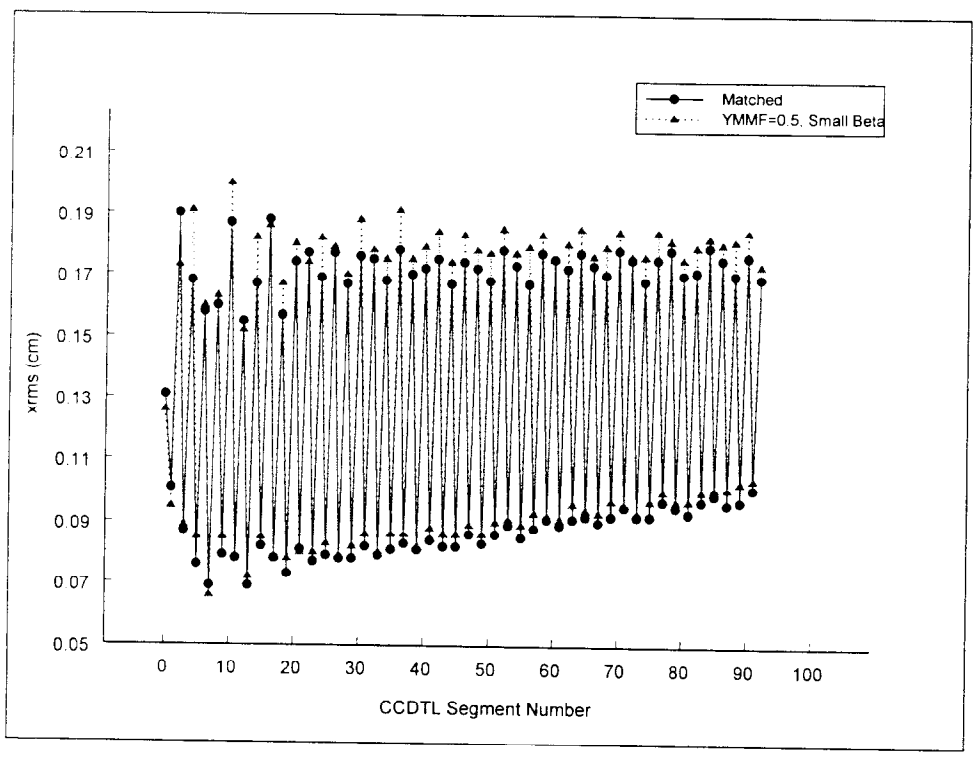

Figure 35 – X-rms beam size as a function of CCDTL segment number for an input beam y-mismatch factor of 0.5 and using the small-β-value.

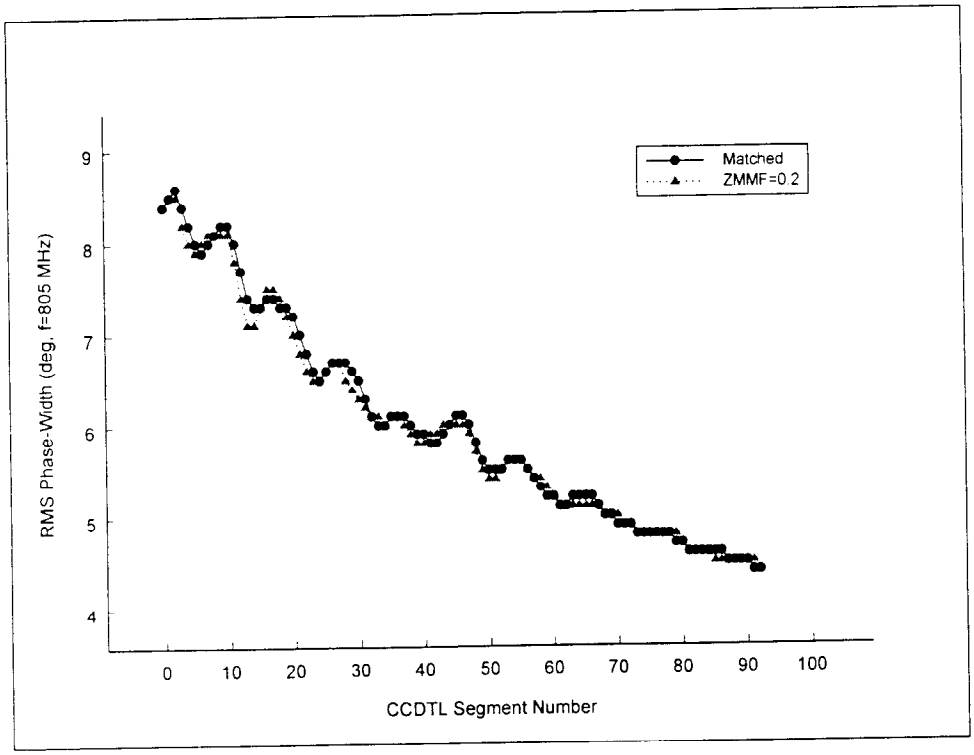

Figure 36 – RMS phase-width in degrees at f=805 MHz as a function of CCDTL segment number for an input beam longitudinal mismatch factor of 0.2.

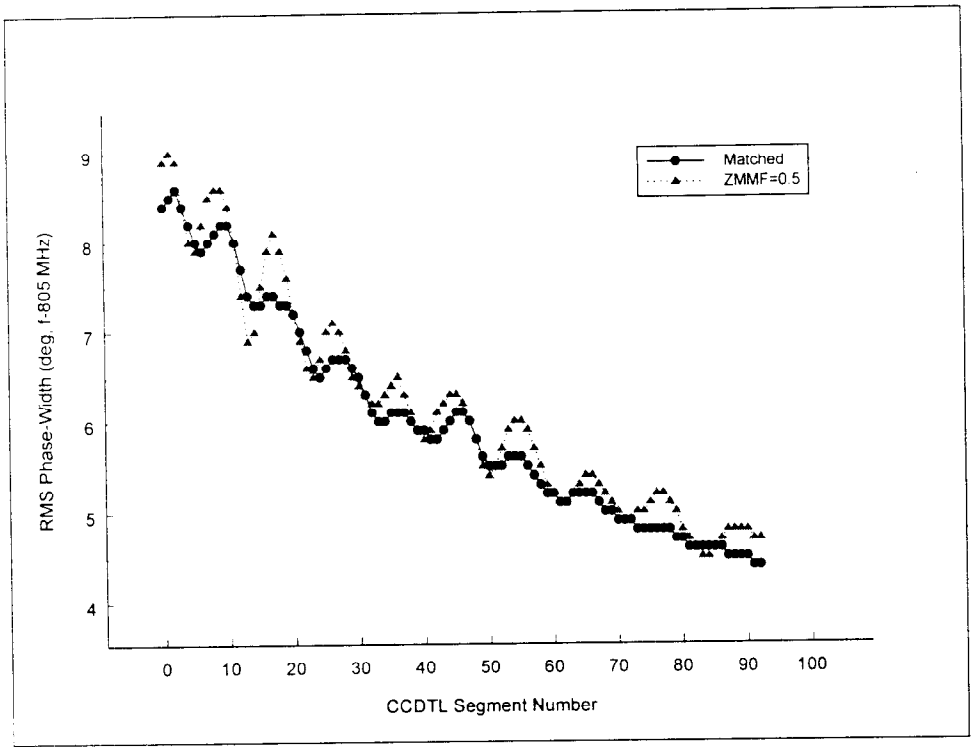

Figure 37 – RMS phase-width in degrees at f=805 MHz as a function of CCDTL segment number for an input beam longitudinal mismatch factor of 0.5.

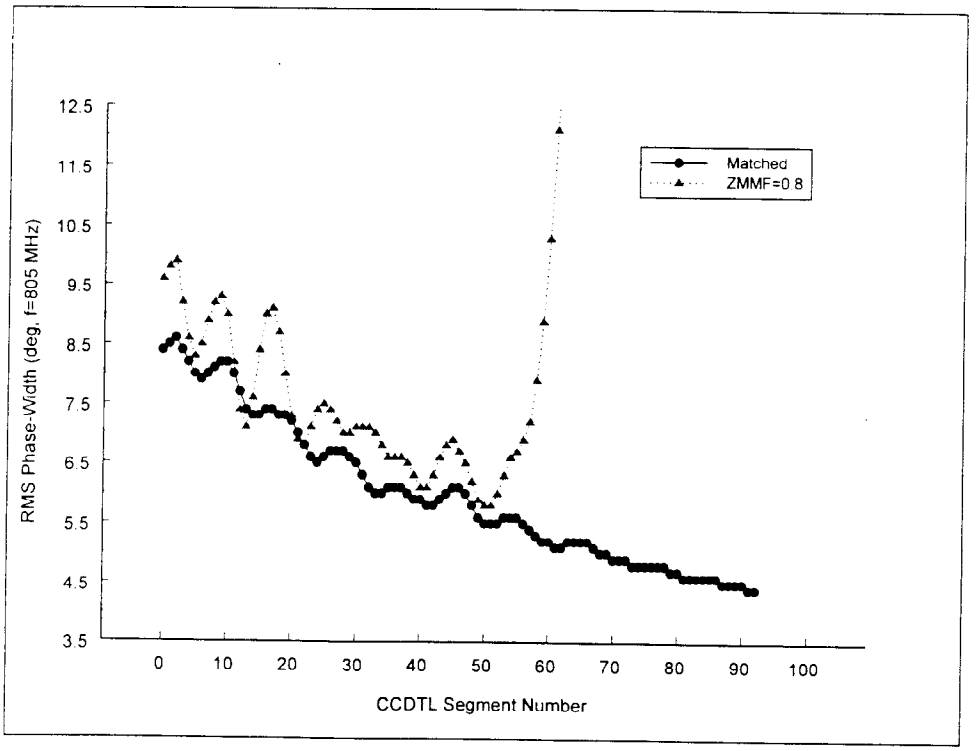

Figure 38 – RMS phase-width in degrees at f=805 MHz as a function of CCDTL segment number for an input beam longitudinal mismatch factor of 0.8.

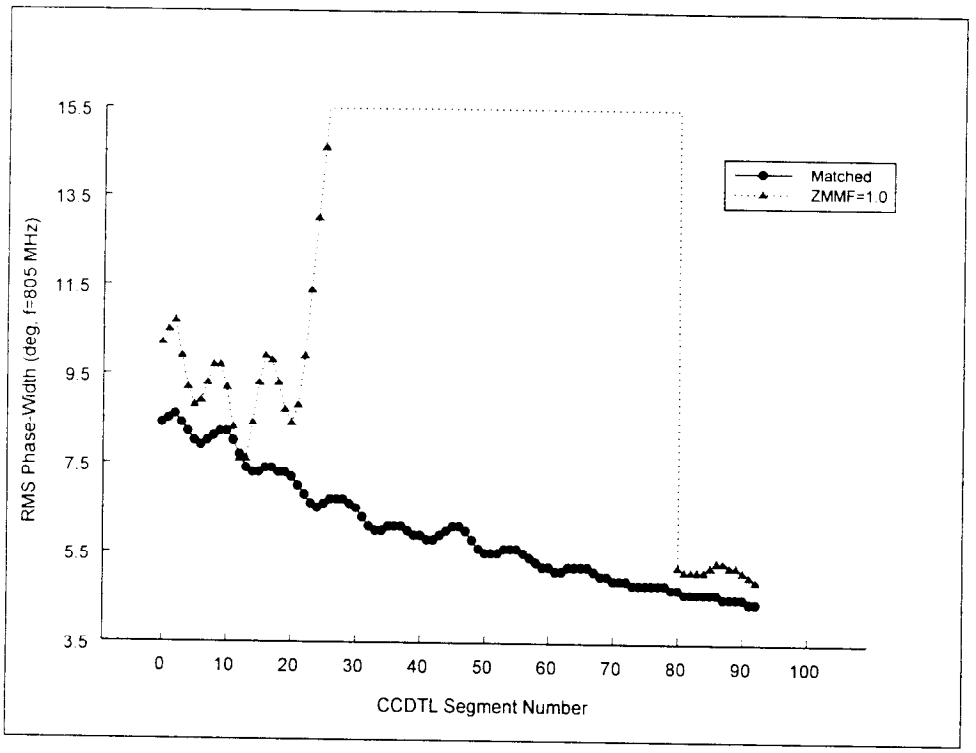

Figure 39 – RMS phase-width in degrees at f=805 MHz as a function of CCDTL segment number for an input beam longitudinal mismatch factor of 1.0.